Predicting the thermal performance of a sand-based seasonal thermal storage

Rebecca I. Pinto[a], Ian Beausoleil-Morrison[a]
[a]Carleton University, Ottawa, Canada

Abstract

A two-storey research house that represents a typical Canadian home has been built and equipped with a solar thermal system and underground seasonal sand thermal storage. A 3D finite difference model of the heat transfer in the sand storage has been developed and the simulation's results are compared to experimental data in order to refine and partially validate the model.

The experimental data shows that the underground seasonal storage is cooling approximately twice as fast as predicted by the numerical model. Analysis of the experimental data has led to a hypothesis for the rapid heat loss and recommendations to adapt the numerical model to better predict the experimental data.

Introduction

In 2016, space heating (SH) and domestic hot water (DHW) heating for Canadian residential buildings accounted for over 75% of residential energy use and 11% of Canada's total GHG emissions (Statistics Canada, 2019; Environment and Climate Change Canada, 2018; National Resources Canada, 2016). In order to drastically decrease the GHG emissions from the residential sector, solar thermal energy, harnessed by solar thermal panels, can be used to partially or totally fulfill the SH and DHW needs of residential buildings.

One of the biggest challenges in capturing and using solar energy in high latitude locations like Canada, is the timing mismatch between the solar radiation received and the space heating needs of homes. For example, a high percentage of annual solar energy is incident during the summer months, when heating demand in buildings is low; the converse is also true. A seasonal thermal energy storage (STES) bridges this gap by storing thermal energy when it is readily available and discharging it when the thermal demand arises (Cruickshank and Baldwin, 2016). By using an STES to harness solar energy for DHW and SH, this technology has the potential to reduce the dependence of Canadian housing on fossil fuels and dramatically reduce the sector's GHG emissions.

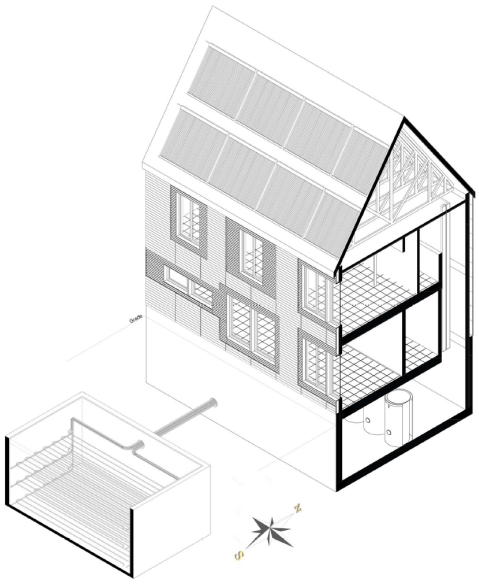

Figure 1: Urbandale Centre for Home Energy Research, with adjacent seasonal thermal sand storage.

Previous research suggests that buildings connected to solar thermal systems with district-level seasonal storage can use solar energy to achieve 90% to 100% of their annual space heating needs (Sibbitt et al., 2012). For residential-scale STES, there are only a few of these types of studies in current literature. Additionally, they use either water as an STES medium or an adsorption-based STES (Beausoleil-Morrison et al., 2019). Mahfoudi et al. (2014) showed that sand can be used for solar thermal storage, but no research has yet been published demonstrating the efficiency of a sand-based STES for a residential building. Using this type of technology would be more cost-effective than a water-based STES, if it can be proven. In order to demonstrate that a sand-based STES could meet residential SH and

DHW needs with solar energy, full-scale experimental research has been conducted at the Urbandale Centre for Home Energy Research (CHEeR), a research house in Ottawa, Canada, equipped with solar thermal collectors and an underground seasonal thermal sand storage (Figures 1 and 2).

As a step in demonstrating the relevance of a sand-based STES, a three-dimensional (3D) numerical model of the heat flows into and out of the sand STES has been developed and compared with experimental data to validate the model. This paper will describe the development and partial validation of the numerical model that represents the interactions between the seasonal sand storage and the surrounding ground; therefore, the CHEeR house and its solar thermal system will not be described. Interested readers are directed towards Meister and Beausoleil-Morrison (2021), in which a detailed description of the house and its solar thermal system is found.

Physical description of seasonal sand STES

The solar thermal system at the CHEeR house is connected to an underground STES, filled with construction-grade sand and saturated with water. The sand-based STES acts as a battery for thermal energy, storing excess solar energy collected by the CHEeR house's solar thermal collectors during the warmer months, and transferring the stored energy back to the house during the heating season.

The sand STES is a multi-layered cubic prism with an inner core of construction-grade saturated sand (6m x 6m x 3m [LxWxH]). It is surrounded by a 0.35m layer of R-70 extruded polystyrene (XPS) insulation on all four vertical sides, and a layer of R-70 expanded polystyrene (EPS) insulation on its top and bottom, a material which can resist more compressive loading than the XPS insulation. Moving outward from the insulation layer, there is a structural layer of 0.1 m-thick concrete, supporting the bottom face and the four vertical walls. The insulation and concrete layers are separated from both the inner sand STES and the surrounding soil by two impermeable membranes (pool liners), designed to prevent the migration of water across its barriers. The sand STES's top insulation layer is located 1.5 m below grade. Figure 2 shows the sand STES under construction, and Figure 3 shows a cross-sectional illustration of the sand STES's layers and the surrounding soil.

Heat is transferred between the sand STES and the CHEeR house via a bundle of cross-linked polyethylene (PEX) tubing (Figure 1); the working fluid is city water. To distribute the heat throughout the sand STES, three horizontal layers of PEX tubing run through it

Figure 2: Seasonal thermal sand STES adjacent to CHEeR, under construction.

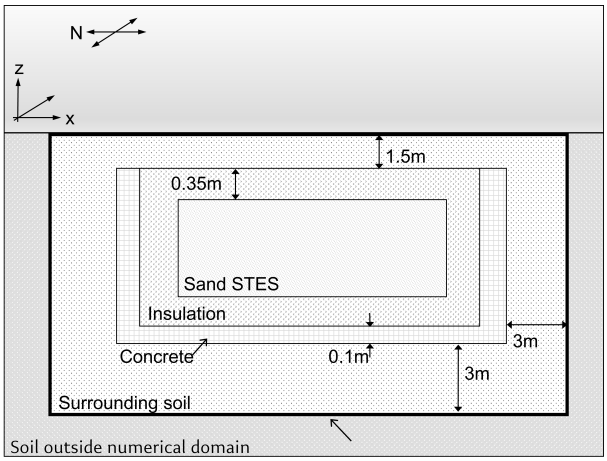

Figure 3: The sand STES, its surroundings layers, and the boundaries of its numerical model's domain; cross-section in the x-z plane.

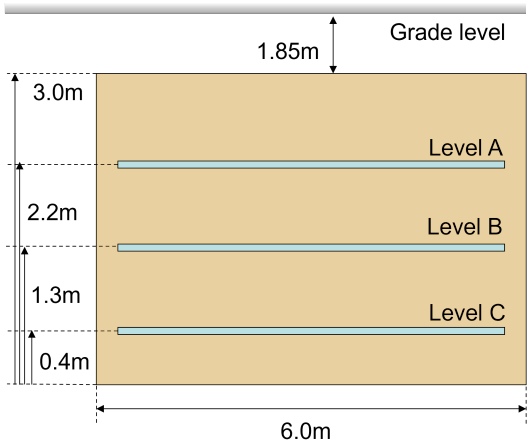

Figure 4: Elevations of PEX tubing and instrumentation within sand STES; cross-section in x-z plane.

in a serpentine layout, at the three elevations indicated in Figure 4 (Levels A, B, and C). The total length of supply and return PEX tubing in the sand STES is approximately 945 m, and the tubing layout was designed to maximize heat transfer to the sand STES, while minimizing parasitic heat losses to the return piping.

Instrumentation

There are 108 thermocouples (TC) in the sand STES, made from Type-E TC wire, and thirty-six TCs have been placed at each of the elevations shown in Figure 4. Their configuration at each elevation is identical and is illustrated in Figure 5. There is a horizontal distance of one metre between each TC, and a horizontal distance of 0.5 m between each outer TC and the closest sand STES wall.

There are 12 volumetric moisture sensors distributed between the sand STES's three levels. The four sensors at Level A are located at positions A22, A25, A52, and A55 (Figure 5), and the configuration of the four sensors at the other two levels is identical.

Numerical model of seasonal sand STES

A finite difference (FD) method has been selected as an appropriate numerical method for this system because the nature of the heat transfer processes can adequately be captured with this method. Cichota et al. (2004) compared FD solutions to analytical solutions for heat transfer in different soils, and found it an appropriate numerical method. A literature search also shows that FD methods have been used to model soil heat transfer by many research groups, including Lee and Lam (2008) and Ngo and Lai (2009).

The sand STES has been represented as a 3D finite difference model (FDM), in Cartesian coordinates, with the origin of the coordinate system at the north-west

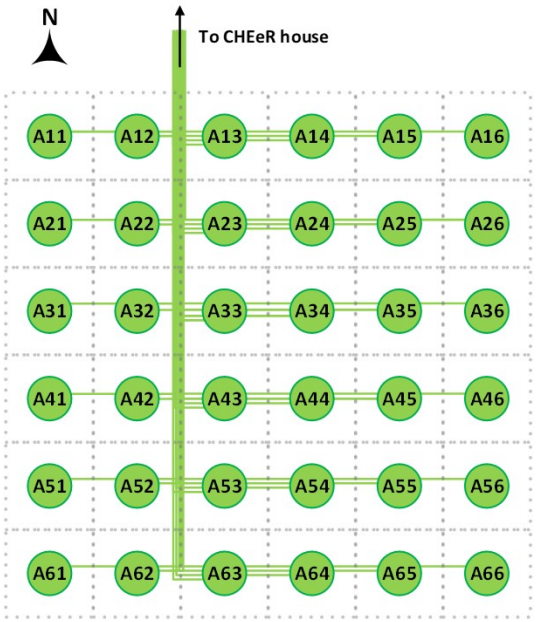

Figure 5: Configuration of thermocouples at Level A of the sand STES.

bottom corner of the sand STES. The numerical domain consists of the sand STES (including its insulation and concrete layers) and a three-metre layer of ground soil on all sides, except at the top face, which only has a 1.5 m layer of soil above the sand STES (Figure 3).

Exclusion of convection in the numerical model

The sand STES was saturated with water during its construction (Figure 2, bottom image); therefore, it is possible that convection is an important mode of heat transfer within the sand STES. At the outset of the research, a hypothesis was made that a conduction-only numerical model would be adequate to predict performance and improve the design of a seasonal sand STES coupled with a solar combisystem. The model's performance would be compared to experimental data to determine if a conduction-only model was a valid hypothesis.

Fortunately, the moisture sensors in the sand STES ended up provding preliminary evidence that supported the conduction-only hypothesis. During the experimental research period, the temperature of the STES varied from approximately 20°C to approximately 70°C. If convection were a significant mode of heat transfer within the sand STES, at higher temperatures we would expect to see moisture transferred from the lower levels of the sand STES to its upper levels. Table 1 lists volumetric moisture content readings within the sand STES at two different temperatures. Since we do not see moisture transfer from lower to upper levels at the higher temperature, we can conclude that convection

Table 1: Volumetric moisture contents of the three STES levels, at different average STES temperatures.

Avg. STES temp. ($^{\circ}C$)	Moisture content (vol %)		
	Level A	Level B	Level C
26	7	10	32
65	8	16	36

is not a significant mode of heat transfer in the sand STES.

There is a curious trend in Table 1, however. All three sand STES levels have higher volumetric moisture content readings at the higher temperature than at the lower temperature. It seems impossible that the total amount of water within the sand STES is increasing at higher temperatures and decreasing at lower temperatures. However, the phenomenon can be explained by the way in which the moisture sensors measure volumetric moisture content, and the inverse relationship between water viscosity and temperature. At higher temperatures, water has a lower viscosity, which allows it to penetrate deeper into the pores between the sand grains. This increases the dielectric permittivity of the bulk sand medium, which increases the speed of the electric signal between the moisture sensor's probes, and causes the sensor to register a higher value for the volumetric moisture content even though the total amount of water in the area has not changed (Campbell Scientific, 2015). This phenomenon therefore explains the values observed in Table 1.

Assumptions used in numerical model

- The thermal conductivities, densities, and specific heat capacities of the system's materials are assumed to remain constant over time, and are assumed to be the values listed in Table 2. These values are either taken from literature or manufacturer's specifications. They are assumed to be constant over time because there is not enough data available in the literature to calculate these thermal parameters as a function of temperature or time (material aging).
- The sand is vertically stratified into three sections, each with a different water volume content (top/middle/bottom: 7/11/33 vol%). Within each section, water volume content, thermal conductivity, density, and specific heat capacity, are assumed to be uniform. This assumption is based on observed readings of the moisture sensors installed in the sand STES.
- The boundaries of the numerical domain are at undisturbed ground soil temperatures, and vary according to the Kusuda-Achenbach equation as a function of depth below surface (Kusuda and Achenbach, 1965). Boundary temperatures are time-variant and updated every seven days of the simulation.
- Weather effects at grade level, such as solar irradiation, precipitation, and snow cover, as well as the latent heat of soil freezing/thawing, are not taken into account in the numerical model. The ground surface temperature is calculated as described in the previous bullet—calculated using the Kusuda-Achenbach equation and updated every seven days.

Table 2: Thermal parameters of materials in numerical model.

Material	λ (W/mK)	C_p (J/kgK)	ρ (kg/m^3)
Soil	2	750	2800
Concrete	1.4	880	2300
Insulation	0.0288	1500	30
Sand (top)	0.6	952	1920
Sand (middle)	1.0	1018	1960
Sand (bottom)	2.5	1337	2179

Note: The sand STES layers have different thermal properties due to different moisture contents (see Assumptions section).

Governing equation

The governing equation (GE) for heat transfer in the sand STES is given below. It is a conduction-only model, as indicated in the previous sections.

$$\nabla \cdot (\lambda \nabla T) + \dot{Q}_{gen} = \rho C_p \frac{\partial T}{\partial t} \tag{1}$$

The equation can then be expanded for a 3D system in Cartesian coordinates, becoming:

$$\begin{aligned} &\left(\lambda \frac{\partial^2 T}{\partial x^2} + \frac{\partial T}{\partial x}\frac{\partial \lambda}{\partial x}\right) + \left(\lambda \frac{\partial^2 T}{\partial y^2} + \frac{\partial T}{\partial y}\frac{\partial \lambda}{\partial y}\right) + \\ &\left(\lambda \frac{\partial^2 T}{\partial z^2} + \frac{\partial T}{\partial z}\frac{\partial \lambda}{\partial z}\right) + \dot{Q}_{gen} = \rho C_p \frac{\partial T}{\partial t} \end{aligned} \tag{2}$$

To transform Equation 2 into a FDM, a first-order, forward-difference approximation is used for first derivatives, and a second-order, centered-difference approximation is used for second derivatives. The resulting equation can be written in the explicit form.

A varying mesh size is used for the numerical grid, with a coarser mesh in the ground soil surrounding the sand STES and a finer mesh at certain areas of the sand STES where temperature differences may vary considerably between adjacent nodes.

Initialization of numerical model

The initial conditions (IC) of the model at t=0s are imposed as follows. All nodes in each of the Layers A, B, and C in the sand STES portion of the model are initialized at the same temperature—the averages of the experimental temperature data from the 36 thermocouples of each layer. The boundaries of the numerical domain have their temperatures initialized based on their z-elevation below grade, and are calculated using the Kusuda-Achenbach equation.

The insulation and concrete layers are initialized in three vertical sections, at the average temperature between the sand STES and the average temperature of the vertical boundary layers. Assuming that the soil temperature varies linearly between the concrete and the boundary layers, the soil domain temperatures are initialized on a temperature gradient between those two layers.

The initial conditions across all the layers in the numerical domain are visualized in Figure 6. The blue line marked "IC" shows the cross-section of the ICs imposed across the length of the x-axis, at the midpoints of the y- and z-axes. The pink and grey bands on the figure show where the insulation and concrete cross-sectional layers are located, respectively.

Since the IC temperature profile was manually created and imposed on the model, it may not represent a realistic thermal gradient. Therefore, to start the simulation with temperature distributions that are more representative of realistic thermal gradients, the model has been given a feature called a pre-conditioning period (PCP).

During the PCP, the numerical model starts with the IC temperature profile and then the simulation is allowed to march forward through time, with the sand STES temperatures and the boundary temperatures held constant. The rest of the numerical domain (the insulation, concrete, and soil) is allowed to approach steady-state until the condition $diff < 0.01°C$ is met, where *diff* is the maximum temperature difference between time steps at any node in the numerical domain.

Once this steady-state is reached, the PCP is considered complete. The steady-state temperatures in the numerical domain become the new IC temperatures and the simulation's time counter is reset to t=0s. The simulation is then "restarted" with its new IC temperatures, generated by the PCP. The PCP therefore allows the model's soil, concrete, and insulation layers to have a more realistic set of intial conditions.

The temperature profiles of the numerical domain before and after the PCP are illustrated in Figure 6. Again, temperature profiles were taken across the x-axis, at the mid-points of the numerical domain in the y- and z-directions.

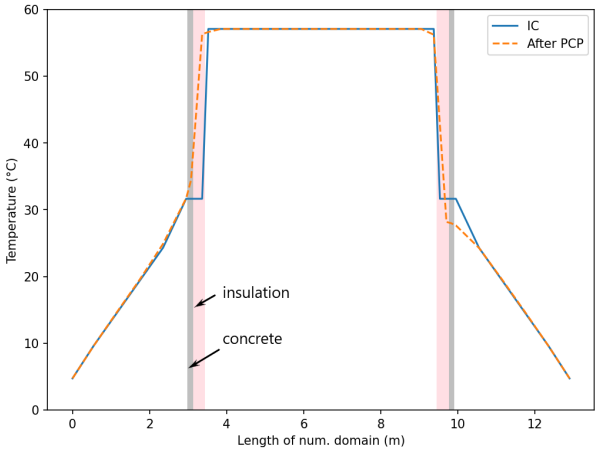

Figure 6: Temperature profiles at t=0s (IC) and after the pre-conditioning period.

Results and discussion

As a first step in validating the numerical model, its simulation results were compared to experimental STES temperatures during a cooldown period that occurred from June to November 2021. A cooldown period occurs when the STES is being neither charged nor discharged[1], and is cooling down according to the temperature difference between it and the surrounding soil.

When the numerical model is run with the thermal parameters listed in Table 2, it is referred to as the base case. Figure 7 shows the experimental temperatures of the STES plotted along with the numerical model's base case predictions. The mean temperatures of each of the three layers of the STES are plotted for each case.

The figure shows that the experimental STES cools down much quicker than the base case numerical model predicts. Since the material thermal properties listed in Table 2 are only estimates of the real-life thermal parameters, a range of plausible values for the different material thermal properties was implemented in the numerical model, to try and match the simulated results to the experimental data. The following are the material thermal parameters that were varied in the parametric simulations:

- the C_p, ρ, and average temperature of the surrounding soil
- the λ, C_p, and ρ of insulation
- the λ, C_p, and ρ of concrete

[1]When the STES is being "charged", heat is being added to it from the house's solar thermal system. When the STES is being "discharged", heat is being withdrawn from it to space heat the house.

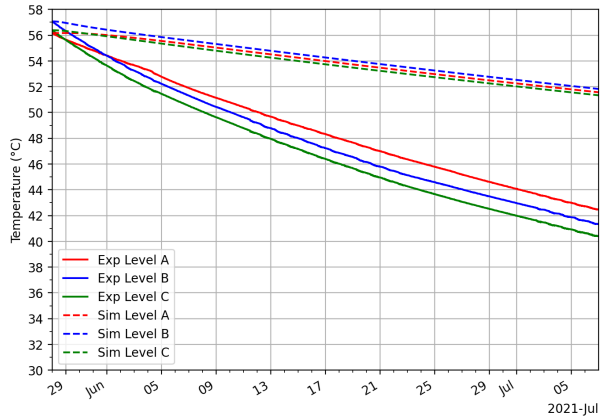

Figure 7: Numerical model temperature predictions (sim) of the base case compared with experimental data (exp); June 2021 cooldown.

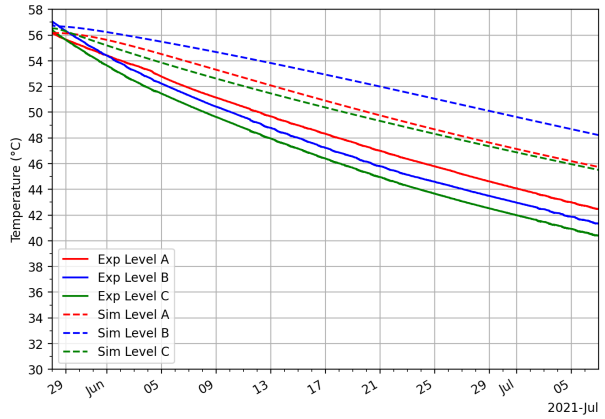

Figure 8: Numerical model temperature predictions (sim) of the "best match" case compared with experimental data (exp); June 2021 cooldown.

- the moisture contents, λ, C_p, and ρ of the sand layers
- the z-elevations of the boundaries between layers of the STES

The simulation attempt that came the closest to the cooling curves of the experimental data (referred to as the "best match" case) is shown in Figure 8. It can be observed that even with the "best match" scenario, the FDM's temperature predictions do not match the experimental cooling curves of the STES—the STES loses substantially more heat than the numerical model predicts.

Investigation of discrepancies

These results were unexpected, so the UA of the STES during the cooling period was calculated using a lumped capacitance approach and compared to that of the numerical model. The sand STES and its walls were treated as cooling uniformly and the average temperature of the surrounding soil was chosen to be the average temperature of the ground in June/July, given by the Kusuda-Achenbach model.

The experimental UA of the STES and the predicted UA of the base case model were calculated to be 20.7 W/K and 11.8 W/K, respectively. Based on the relation for rate of heat transfer $\dot{Q} = UA\Delta T$ (Incropera and DeWitt, 2007), the two UA values indicate that the experimental STES is losing heat almost twice as fast as the rate predicted by the model. Even varying the thermal parameters listed in Table 2 within realistic ranges did not allow the model's predicted temperatures to match the observed experimental temperatures.

The large difference between the experimental and predicted rates of heat loss was unexpected, therefore the experimental data was examined more closely for anomalies that could explain the high experimental UA value.

Figures 9 and 10 show the experimental data, graphed at a finer resolution than in Figures 7 and 8. Each line in each of the three graphs of Figure 9 shows the average temperature of a TC row running east/west in the sand STES (six TCs per row). Similarly, each line in each of the three graphs of Figure 10 shows the average temperature of a TC column running north/south in the sand STES (six TCs per column). Refer to Figure 5 for TC row and column numbering.

Figure 9 shows that that Rows 1 and 2 are noticeably colder that the rest of the rows, on average. Row 1 is by far the coldest row on average, and although Rows 1 and 6 are both equidistant from the outer walls of the STES, Row 1 is much cooler than Row 6 in all three layers of the STES. In fact, in the middle layer of the STES, Row 1 is almost 5°C colder than Row 6 on average. This seems to indicate that the insulation is not performing as expected on the north face of the sand STES, and is likely heavily degraded or damaged.

Similarly, by examining Figure 10, we see that the westernmost column (Column 1) is slightly cooler on average than the other columns of TCs. This indicates that the insulation is not performing as expected on the west face of the sand STES. It does not appear to be performing as poorly as the north face's insulation, but it does still seem to be allowing higher levels of heat loss from the west face of the STES than from its east face.

Figures 9 and 10 therefore indicate that the insulation's thermal conductivity along the north and west faces of the STES will have to be modified to reflect a loss in insulative performance. These changes will be implemented in the numerical model in the next phase of the research plan, and will hopefully bring the model's temperature predictions into congruence with the experimental data.

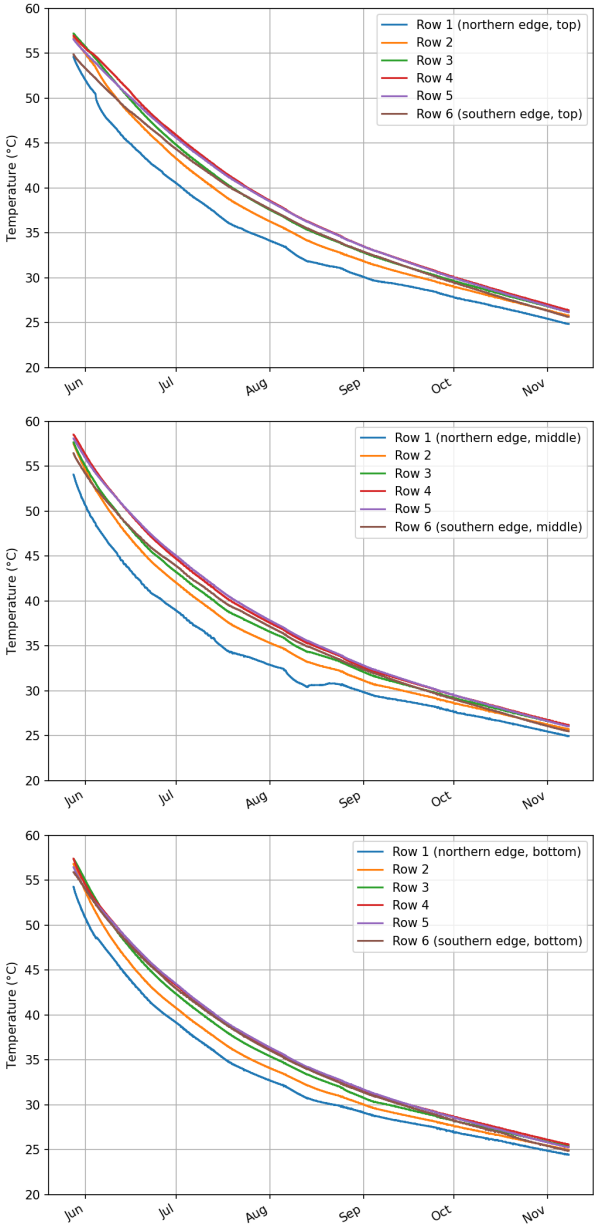

Figure 9: Mean temperatures of east-west TC rows within the top, middle, and bottom layers of the STES; 2021 cooldown.

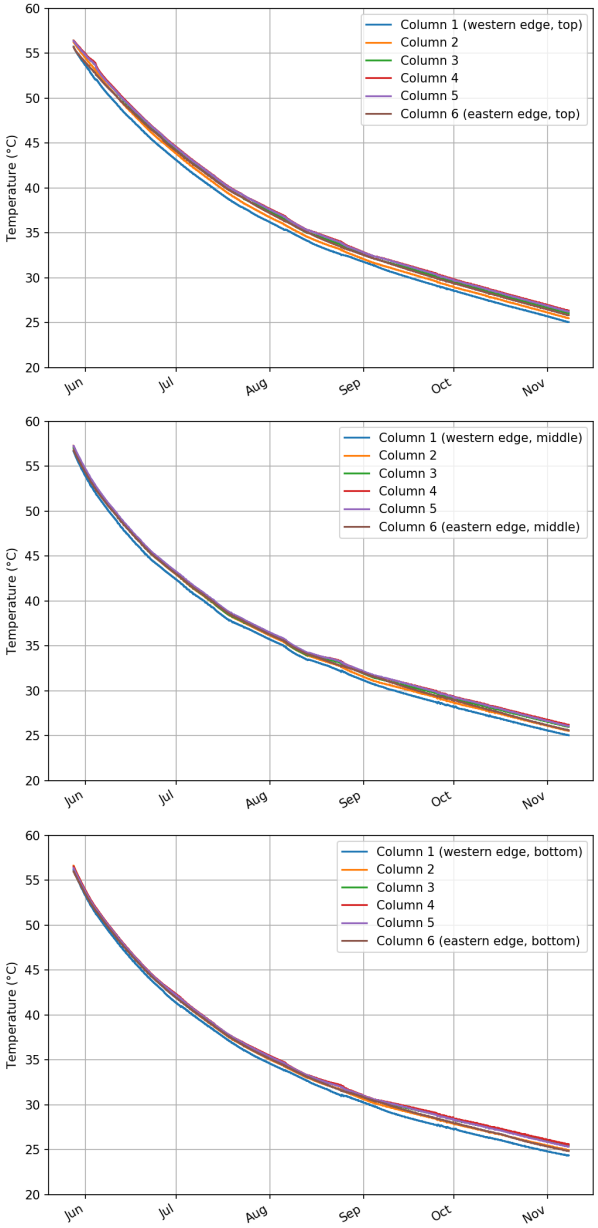

Figure 10: Mean temperatures of north-south TC columns within the top, middle, and bottom layers of the STES; 2021 cooldown.

Conclusion

A 3D finite difference model of a sand-based seasonal thermal energy store was derived and compared to experimental data of the STES to partially validate the model. The assumption of a conduction-only system for the heat transfer model of the sand STES was considered valid since experimental volumetric moisture content measurements did not show moisture migration associated with heat transfer in the sand STES.

The STES's experimental data showed a heat loss rate of almost twice the rate predicted by the numerical model. The experimental data could not be matched by the model's predictions, even when the material thermal parameters were modified. Upon examination of the temperature data from the individual thermocouples in the sand STES, there appears to be some damaged or degraded insulation on the north and west faces of the sand STES. The insulation's thermal parameters will therefore need to be modified in future work to fully validate the model.

Nomenclature

A	area (m^2)
C_p	specific heat capacity ($\frac{J}{kg \cdot K}$)
E	energy (J)
i, j, k	indices for Cartesian coordinate axes, in FDM
n	time step index, in FDM
$\dot{Q}$	rate of heat flow (J/s)
$\dot{Q}_{gen}$	rate of heat generation (J/s)
T	temperature ($°C$)
t	time (s)
U	overall heat transfer coefficient ($\frac{W}{m^2 \cdot K}$)
x, y, z	Cartesian coordinate axes
λ	thermal conductivity ($\frac{W}{m \cdot K}$)
ρ	density (kg/m^3)

References

Beausoleil-Morrison, I., B. Kemery, A. D. Wills, and C. Meister (2019). Design and simulated performance of a solar-thermal system employing seasonal storage for providing the majority of space heating and domestic hot water heating needs to a single-family house in a cold climate. *Solar Energy 191*(May), 57–69.

Campbell Scientific (2015). *Instruction Manual: CS616 and CS625, Water Content Reflectometers*.

Cichota, R., E. A. Elias, and Q. D. J. V. Lier (2004). Testing a finite-difference model for soil heat transfer by comparing numerical and analytical solutions. *Environmental Modelling and Software 19*, 495–506.

Cruickshank, C. A. and C. Baldwin (2016). Chapter 15 - Sensible Thermal Energy Storage: Diurnal and Seasonal. In *Storing Energy*, Chapter 15, pp. 291–311. Elsevier Inc.

Environment and Climate Change Canada (2018). National Inventory Report 1990-2016: Greenhouse Gas Sources and Sinks in Canada.

Incropera, F. P. and D. P. DeWitt (2007). *Fundamentals of Heat and Mass Transfer* (6 ed.). John Wiley & Sons.

Kusuda, T. and P. Achenbach (1965). Earth Temperature and Thermal Diffusivity at Selected Stations in the United States. *ASHRAE Transactions 71*(1), 61–74.

Lee, C. K. and H. N. Lam (2008). Computer simulation of borehole ground heat exchangers for geothermal heat pump systems. *Renewable Energy 33*(6), 1286–1296.

Mahfoudi, N., A. Moummi, and M. E. Ganaoui (2014). Sand as a heat storage media for a solar application: Simulation results. *Applied Mechanics and Materials 621*, 214–220.

Meister, C. and I. Beausoleil-Morrison (2021). Experimental and modelled performance of a building-scale solar thermal system with seasonal storage water tank. *Solar Energy 222*(January), 145–159.

National Resources Canada (2016). Comprehensive Energy Use Database.

Ngo, C. C. and F. C. Lai (2009). International Journal of Heat and Mass Transfer Heat transfer analysis of soil heating systems. *International Journal of Heat and Mass Transfer 52*(25-26), 6021–6027.

Sibbitt, B., D. Mcclenahan, R. Djebbar, J. Thornton, and B. Wong (2012). The performance of a high solar fraction seasonal storage district heating system – five years of operation. *Energy Procedia 30*, 856–865.

Statistics Canada (2019). Report on Energy Supply and Demand in Canada, 2016 revised.